Faraday Discuss., 1995, **102**, 129–146

Resonances and Fluctuations in the Unimolecular Reaction of NO_2

Scott A. Reid, Andrei Sanov and Hanna Reisler

Department of Chemistry, University of Southern California, Los Angeles, CA 90089-0482, USA

Fluctuations and oscillations in the unimolecular reaction of NO_2, and their manifestations in photofragment yield (PHOFRY) spectra, NO rotational state distributions and decomposition rates are examined. Comparisons between experimental and simulated PHOFRY spectra show that extraction of rates from linewidths in state-selected spectra is unjustified in the regime of overlapping resonances. Measurements of the alignment parameter of the NO product in the excess energy range $E^E = 200$–500 cm^{-1} evidence the existence of fluctuations in the decay rate. Changes in the patterns of fluctuations and oscillations in the NO rotational state distributions reveal the progressive tightening of the transition state (TS) as the excess energy increases and the importance of exit-channel interactions beyond the TS. Distributions well fit on the average by phase-space calculations can be obtained even when the transition state is tight.

1. Introduction

The unimolecular decomposition of NO_2 has long served as a prototypical system for addressing experimentally at the state-to-state level many issues central to statistical theories. Experimental studies include: (i) spectroscopic interrogation of vibronic coupling between the ground $1\,^2A_1$ and excited $1\,^2B_2$ electronic states and the exploration of chaos (vibronic and rovibronic) at high excitation energies,[1–12] (ii) measurements of unimolecular reactions rates, $k(E)$ and $k(E, J)$,[13–15] and (iii) determination of detailed product state distributions including vector properties and correlated distributions.[16–37] Although for NO_2 full dynamical calculations on a realistic PES are still beyond reach, significant progress in theoretical descriptions has been made on two fronts: (i) restricted calculations on PESs limited to the region of the TS have yielded realistic descriptions of the unimolecular reaction rates, the vibrational energy distributions, and the correlated spin–orbit distributions,[38–40] and (ii) extension of the random matrix model to the case of overlapping resonances and its application to tight and loose TSs enabled simulations of state-selected photofragment yield spectra, and investigation of the issue of rates *vs.* widths in the case of overlapping resonances.[41,42]

Following much work and some controversy, several aspects of the dissociation of NO_2 are now well established. The dissociation takes place from mixed $1\,^2A_1$–$1\,^2B_2$ states which possess predominantly ground-state character. The near threshold rates at excess energies $E^E = 0$–1500 cm^{-1} ($D_0 = 25\,130$ cm^{-1})[34,36,37] are well described by statistical theories [Rice–Ramspeiger–Kassel–Marcus (RRKM), statistical adiabatic channel model (SACM)].[43–48] The rotational distributions can be fit on the average by phase space theory (PST),[48] and the vibrational distributions and their dependence on E^E are adequately described by variational RRKM theory.[43] The NO and O spin–orbit distributions are on the average colder than statistical.[21,28,29,33] Deviations from statistical predictions appear to be more pronounced at high excess energies (*e.g.* $E^E > 7000$ cm^{-1}).[26,28] Both experimental evidence and theoretical calculations suggest that the TS tightens progressively as E^E increases.

Despite the good agreement (on the average) with statistical models, measurements carried out from well defined initial states and with complete final-state characterization reveal pronounced fluctuations and oscillations.[22,23,28–35] The oscillatory patterns change qualitatively as the excess energy increases, thus providing insights into the decomposition mechanism and the nature of the TS. In this paper we shall emphasize areas of unimolecular dynamics of small molecules that are best revealed through oscillations and fluctuations. In particular, we concentrate on three issues requiring further scrutiny: (i) fluctuations in the state-specific rates and the connection between rates, resonance widths and the observed widths of spectral features; (ii) the effects of averaging and the transition from oscillating/fluctuating state-to-state behaviour to smooth averages; and (iii) exit channel interactions during product evolution; in particular, what statistical theories should internal state distributions be tested against? These general issues will be addressed both by experimental work on NO_2 and by illustrative calculations that qualitatively capture salient features of specific observations.

2. Experimental

A 0.5% or 4% NO_2–He mixture at 1200 Torr was expanded into a vacuum chamber [evacuated to *ca.* (2–3) $\times$ 10^{-6} Torr] *via* a piezoelectrically actuated pulsed nozzle (0.5 mm diameter orifice, 180 μs pulse duration).[29–32] The molecular beam was intersected *ca.* 15 mm downstream from the orifice by collinear and counter-propagating photolysis and probe laser beams, each produced from an excimer laser pumped dye laser system. For the alignment measurements, tunable radiation at $\lambda = 398$–370 nm (QUI/dioxane) was used for photolysis, and typical pulse energies were *ca.* 1–5 mJ in a 2–3 mm diameter beam. The double-resonance excitation scheme has been described in detail elsewhere.[32] In this method, specific rotational states in the ($101 \leftarrow 000$) band of NO_2 were excited with tunable IR radiation from an $LiNbO_3$ optical parametric oscillator (OPO), and the vibrationally excited molecules were further excited with a tunable laser to energies above D_0. Tunable radiation at $\lambda = 224$–227 nm, generated by frequency doubling the fundamental dye output (C450/methanol) in a BBO crystal, was used to excite NO fragments on the diagonal bands of the γ-system. Fluorescence collected by a three-lens telescope[32] was imaged through a 'solar blind' filter onto the surface of a photomultiplier tube (PMT, Hamamatsu RU166H). To avoid partial saturation of the strong NO transitions, which is important for alignment and product distribution measurements, typical probe pulse energies were kept at 0.1–0.5 μJ in a 5 mm diameter beam. For other experiments, probe energies ≤ 40 μJ were used.

Three types of experiments were carried out. First, state-specific one-photon or IR–visible PHOFRY spectra were obtained by scanning the photolysis laser frequency while probing a specific NO quantum state.[30–32] Secondly, NO product state distributions were determined by fixing the photolysis laser and scanning the probe laser.[29,31] Finally, alignment measurements of the NO fragment at specific photolysis wavelengths were obtained. Here the polarization of the nominally vertically polarized photolysis beam was further purified by a Rochon prism polarizer before passing through a photoelastic modulator (PEM) configured to rotate the plane of polarization by 90° on alternate laser shots. This allowed direct shot-to-shot collection of signal for parallel and perpendicular photolysis/probe polarizations. Typical polarization extinction ratios of >100 were obtained as measured by a pyroelectric detector (Molectron J3-05) before the chamber entrace window. At each photolysis wavelength, typically (1–2) $\times$ 10^5 laser shots were averaged at each laser polarization.

3. Widths of Spectral Features in the Case of Overlapping Resonances

Recently, it has become possible to observe the manifestations of overlapping resonances in state-to-state unimolecular reactions. When resonances overlap and interact *via* a

common continuum, they interfere and such interference will modify the lineshapes and positions, giving rise to asymmetric lineshapes.[49–53] Above D_0, each resonance has a characteristic width, and in unimolecular reactions several resonances often overlap.[54] By monitoring specific final states of the products, partial absorption spectra [*i.e.* the so called PHOFRY, photofragment excitation (PHOFEX), or action spectra] can be obtained. If the final states are largely uncorrelated, each may derive from a slightly different combination of resonance amplitudes and phases (for a fixed photolysis energy), giving rise to a somewhat different interference pattern and thus different lineshapes. This is precisely what is observed in the state-specific PHOFRY spectra of NO_2.[30–35] Examples of representative PHOFRY spectra obtained at excess energies E^E = 2000–2500 cm^{-1} by monitoring different NO product states are shown in Fig. 1.

The PHOFRY spectra can be qualitatively simulated using a model based on assumptions inherent in statistical theories, *i.e.* the parent eigenstates are ergodic and formation and decay of the activated complex have uncorrelated phases.[32,41,42] Consequently, the parent nearest neighbour level spacings are assumed to obey a Wigner-like distribution.[1,6,10] Since the parent wavefunctions can be described with a basis set of normal modes with random coefficients, we also assume that, in analogy with the case of isolated resonances, the coupling matrix elements to the continuum of fragment channels are random, and that this in turn leads to randomly fluctuating resonance widths obeying a chi-square-like distribution with n degrees of freedom. Here, n is the number of states independently coupled to the zeroth-order levels;[55–57] for a loose TS n equals

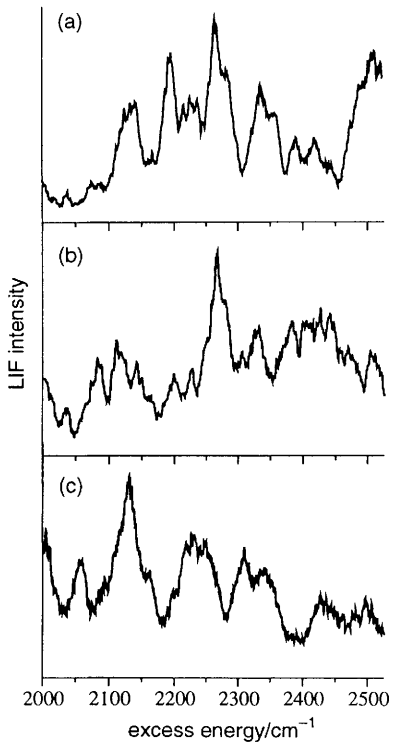

Fig. 1 Representative NO_2 IR-visible PHOFRY spectra at E^E = 2000–2525 cm^{-1} obtained by monitoring (a) NO(v = 0) Q_{11}(33.5) and (b) R_{22}(23.5) transitions, and (c) NO(v = 1) R_{11}(7.5) transition

the number of open fragment channels, while for a tight TS n is the number of energetically accessible states of the TS. The amplitude of each resonance, $R_m(E)$, is given by:[32,42,49]

$$R_m(E) = \frac{a_m\sqrt{(\Gamma_m/2\pi)}}{(E - E_m) + (i\Gamma_m/2)} \tag{1}$$

where E_m is the resonance energy, a_m is the resonance excitation amplitude and Γ_m is the sum of the partial widths of the resonance m into all final channels f. The coefficient $\sqrt{(\Gamma_m/2\pi)}$ ensures normalization, *i.e.*, $\int_{-\infty}^{\infty} |R_m(E)|^2 \, dE = a_m^2$. In the case of isolated resonances, Γ_m can be measured directly from the linewidth and is related to the decay rate $k(E)$ by the uncertainty principle, $\Gamma_m = hk(E_m)/2\pi$. In contrast, when the resonances overlap, the decay width is an unobservable quantity, and the relationship between $\langle\Gamma(E)\rangle$ (the average decay width) and $k(E)$ is not simple.[41,42,58]

The goals of the present simulations are: (i) to demonstrate the correlation between the partial and total spectra under conditions similar to those used in recent state-to-state experiments on the decomposition of NO_2,[30–32] and (ii) to explore the relationship between the resonance width and the widths of individual spectral features. This is important since extraction of decay rates from line widths is often attempted. In the calculations described by Peskin *et al.*[41,42] as well as here, a_m are chosen as uniform random deviates and the nearest-neighbour level spacings of the resonances obey a Wigner-like distribution. We use a chi-square distribution of decay widths in our simulations,[32] despite the fact that Peskin *et al.* demonstrated a progressive deviation from this form as the degree of resonance overlap increases.[42] We find that for a fixed $\langle\Gamma(E)\rangle$, the simulations are not sensitive to the exact form of the width distribution.[32,42]

It has been shown that for a given set of resonances (*i.e.* for pre-selected arrays of E_m, a_m and Γ_m) the probability of producing a final state f at energy E, $P_f(E)$, is given by the general form:[32,42]

$$P_f(E) = \left| \sum_m R_m(E) \cdot C_{fm} \exp(i\phi_{fm}) \right|^2 = \left| \sum_m \frac{a_m \cdot C_{fm} \exp(i\phi_{fm})\sqrt{(\Gamma_m/2\pi)}}{(E - E_m) + (i\Gamma_m/2)} \right|^2 \tag{2}$$

where the amplitudes C_{fm} and phases ϕ_{fm} defining the projection of the resonance m on the final states f are real numbers taken as uniform random deviates in the intervals 0–1 and 0–2π, respectively. This expression has been recently obtained from a random matrix version of Feshbach's optical model, where the coupling of the TS to the molecular complex is modelled *via* a universal random matrix effective Hamiltonian.[42] This Hamiltonian matrix, whose diagonalization provides the resonance eigenstates and widths and describes correctly the average unimolecular decay rate,[41,42] can be used in both loose and tight TS cases.[42] The simplified description of eqn. (2) yields spectra qualitatively similar to ones obtained by the more rigorous treatment of Ref. 41 and 42.

The simulated spectra are compared to experimental PHOFRY spectra obtained in two excess energy regimes: $E^E = 2000$–2525 and 475–650 cm^{-1}.[30,32] The PHOFRY spectra still contain some averaging despite full NO($^2\Pi_\Omega$; v, J, Λ) quantum state specificity; *i.e.* we average over the three spin–orbit states of the correlated atomic oxygen fragment ($j = 2, 1, 0$), as well as over several parent rotational states. (Even with double-resonance excitation it was not possible to excite a single rotational state of NO_2.)[32] For $E^E = 2000$–2525 cm^{-1}, we have recorded PHOFRY spectra for 15 different NO final states,[32] and some of these spectra are shown in Fig. 1. Although not all populated NO product channels have been monitored, qualitative conclusions about the total absorption spectrum can be drawn by summing these 15 spectra (Fig. 2). Clearly, the main effects of summation are: (i) an increase in background, (ii) broadening of the peaks, and (iii) a decrease in the range of widths in the summed spectrum. We note that based on the reactive density of states there should be *ca.* 250 resonances in this

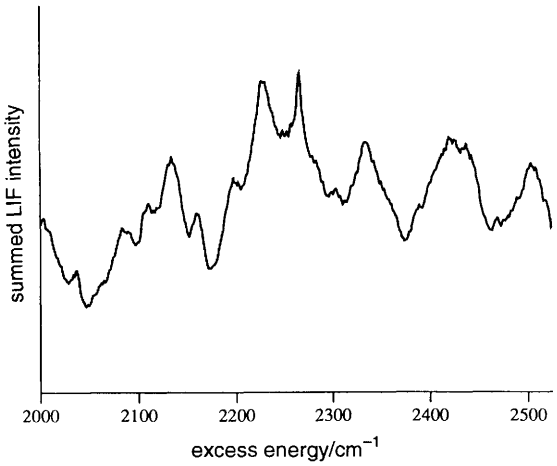

Fig. 2 NO_2 IR-visible yield spectrum obtained by summing 15 individual PHOFRY spectra of NO($v = 0, 1$; J) obtained at $E^E = 2000$–2525 cm^{-1}

region;[10,11,35,59] yet fewer than *ca.* 20 peaks are observed in either partial or total spectra. It is intriguing that residual structure is apparent in the summed spectrum despite the extensive averaging of seemingly rather different spectra, suggesting the spectra are correlated.

In order to simulate PHOFRY spectra in a given energy range, we use eqn. (2) with a pre-selected random set of resonances, whose number reflects the vibronic density of states (ρ). Resonance widths (with average $\langle\Gamma\rangle$) are assigned from a chi-square-like distribution with n degrees of freedom, where n is the number of energetically accessible TS levels or independent decay channels. Since in the regime of overlapping resonances the decay rate $k(E)$ is not related to $\langle\Gamma\rangle$ simply by the uncertainty principle,[41,58] the RRKM equation is not used here, and $\langle\Gamma\rangle$, ρ and n are treated as independent parameters taken either from calculations, [38,60] or chosen to fit experimental data.[11,29–35] To simulate the spectra shown in Fig. 1, we use $n = 20$, $\langle\Gamma\rangle = 25$ cm^{-1} and $\rho = 0.5$ per cm^{-1}. The simulations are less sensitive to n and ρ and more sensitive to $\langle\Gamma\rangle$.

Given a set of resonances, each array of random coefficients C_{fm} and ϕ_{fm} in eqn. (2) generates a synthetic PHOFRY spectrum for a single fully quantum-state-resolved decay channel. To account properly for experimental averaging over oxygen spin–orbit states and parent rotational states, nine single-channel spectra are used to simulate PHOFRY spectra for individual NO quantum states. First, spectra weighted to simulate the contributions from the three spin–orbit states of oxygen are summed. The average spin–orbit ratios are $^3P_2 : {}^3P_1 : {}^3P_0 = 1 : 0.2 : 0.04$ at $E^E \approx 2000$ cm^{-1}.[21,33] However, since these ratios are known to fluctuate about this average,[33] we assign them at random from the interval c_j/g-$c_j g$ were c_j is the average spin–orbit ratio and g is the fluctuation parameter, which is assumed to be 3. Secondly, three spectra thus summed over the oxygen spin–orbit contributions are averaged to account for incoherent averaging over parent rotational states in the double-resonance experiments.[32] Several representative synthetic spectra are shown in Fig. 3, and the sum of 15 such spectra is shown as the solid line in Fig. 4. Note the qualitative similarities between the simulated and experimental spectra in terms of the number of peaks, range of widths and the differences among individual spectra.

Since the number of summed spectra represented in Fig. 4 is large, it is instructive to see the effect of incoherent superposition of the underlying 250 resonances in this spectral region, *i.e.*

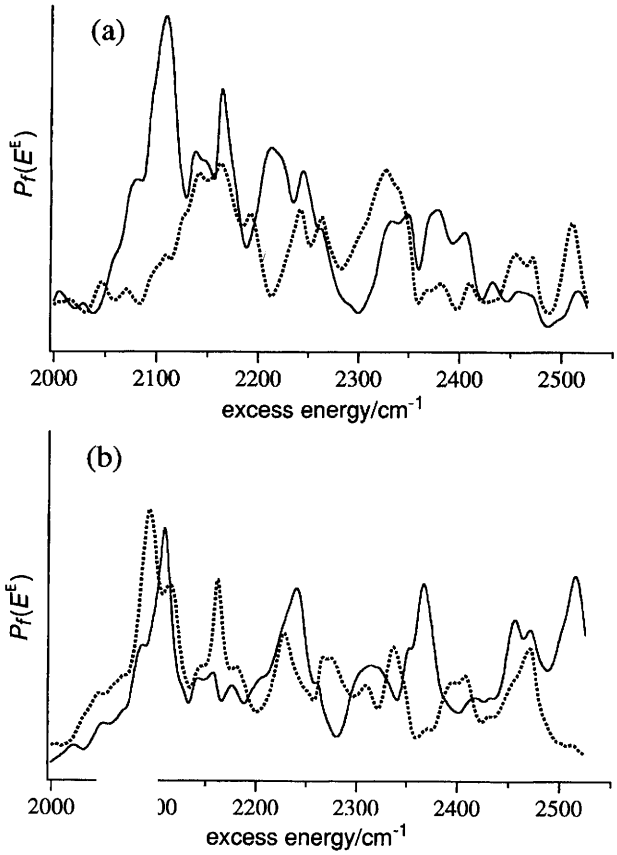

Fig. 3 Four representative simulated spectra corresponding qualitatively to IR-visible PHOFRY spectra of NO_2 at $E^E = 2000$–2525 cm^{-1}. The parameters used in the simulations, $n = 20$, $\langle\Gamma\rangle = 25$ cm^{-1}, and $\rho = 0.5$ per cm^{-1}, have been chosen to simulate best the experimental PHOFRY spectra. The level of incoherent averaging included in the calculated spectra corresponds roughly to that involved in the experimental IR-visible spectra when monitoring a single NO level.

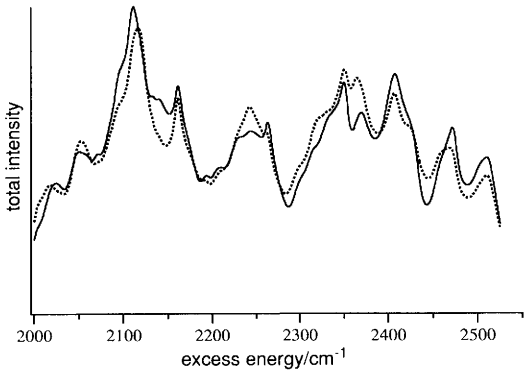

Fig. 4 Solid line: sum of 15 individual simulated spectra such as those shown in Fig. 3. Dotted line: spectrum obtained by incoherent superposition of the resonances used in calculating the simulated spectra [eqn. (3)].

$$I(E) = \sum_m |R_m(E)|^2 = \sum_m \frac{a_m^2 \Gamma_m/2\pi}{(E - E_m)^2 + (\Gamma_m/2)^2} \quad (3)$$

The incoherent superposition is generated by the single sum given by eqn. (3), and is shown as the dotted line in Fig. 4. The two spectra in Fig. 4 are quite similar, indicating that the summation of 15 individual spectra is sufficient to largely average out the effects of phase and interference. Thus, although some differences between the coherent and incoherent superpositions can still be discerned, the random-phase approximation is justified at this level of averaging.

Using eqn. (2), we have successfully simulated the experimental PHOFRY spectra in other regions of excess energy.[32,42] In most cases, when a large number of spectra are summed the result reproduces quite well the spectra obtained by incoherent superposition of the underlying resonances, in a similar manner to the spectra shown in Fig. 4.

In spectra such as those shown in Fig. 3 and 4, as well as in others with $\langle\Gamma\rangle\rho > 5$, it is clear by inspection that the resonances are indeed overlapped. The situation is more ambiguous for smaller overlap. Take for example the synthetic spectra simulating the region close to threshold. Fig. 5(a) displays two simulated spectra that correspond qualitatively to PHOFRY spectra in the region $E^E = 100$–300 cm^{-1}. The parameters in these simulations are $n = 8$, $\rho = 1$ per cm^{-1} and $\langle\Gamma\rangle = 3$ cm^{-1}. The individual spectra exhibit some differences, yet the sum of 15 such spectra still displays many sharp spectral

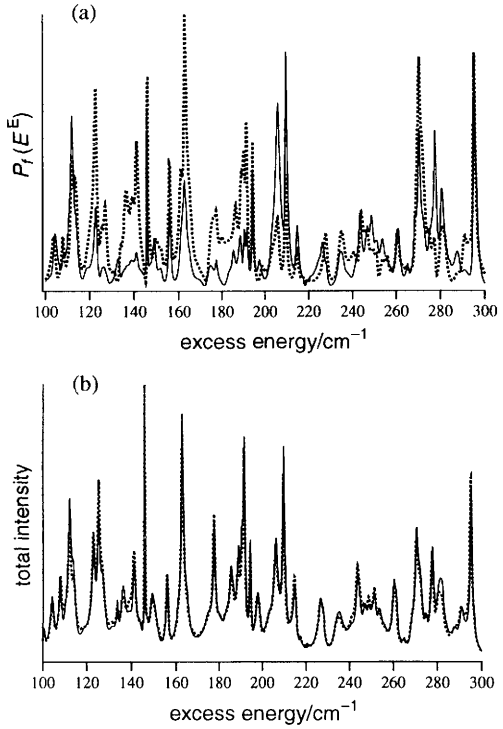

Fig. 5 (a) Two representative simulated spectra corresponding qualitatively to IR-visible PHOFRY spectra of NO_2 at $E^E = 100$–300 cm^{-1}. The parameters used in the simulations are $n = 8$, $\langle\Gamma\rangle = 3$ cm^{-1}, and $\rho = 1$ per cm^{-1}. (b) Solid line: sum of 15 individual simulated spectra such as those in panel (a). Dotted line: spectrum obtained by incoherent superposition of the resonances used in calculating the simulated spectra [eqn. (3)].

features, as shown in Fig. 5(b). Note that for this lower degree of overlap, both the summation of the individual spectra and the incoherent superposition of the 225 underlying resonances produce similar results; *i.e. ca.* 30 peaks, many of which appear rather narrow. It is instructive therefore to extract 'widths' for these spectral features by treating them as single Lorentzians. The average width of the individual spectral features is 1.8 ± 0.1 cm^{-1} in the state-selected spectra and 2.6 cm^{-1} in the summed spectrum, a substantial broadening. The average widths obtained from features in the state-specific spectra are thus much narrower than the input average width (3 cm^{-1}), reflecting both the effects of interference and a bias in favour of narrow peaks when selecting peaks that appear 'isolated'. Similar behaviour is observed in the experimental results. For example, PHOFRY spectra obtained with double-resonance excitation exhibit a greater number of narrow features than those obtained with one-photon excitation.[32,54] Also, spectral features in PHOFRY spectra obtained by monitoring the O fragment are on average broader than those obtained by monitoring single NO states.[21,31,32,35] This reflects the fact that the former arise from superposition of spectra correlating with many NO states.[54]

We also point out that Peskin *et al.* have recently shown that when resonances overlap, the average width cannot be linearly related to the average rate, but in fact the calculated rate is always smaller than that inferred from the average width.[41] Thus, in the regime of overlapping resonances (*i.e.* beyond the tunnelling regime) it is unjustified to extract average unimolecular decay rates from the widths of spectral features, even when many features in the state-specific spectra appear sharp and 'isolated'.

In summary, both the experimental PHOFRY spectra and the simulated spectra show clearly the effects of interference due to overlapping resonances. These effects manifest themselves as marked differences among spectra obtained for different NO final states. The widths of the spectral features in general do not correspond to the widths of the underlying resonances. Summation of a sufficiently large number of PHOFRY spectra yields a spectrum similar to that obtained by incoherent superposition of all the underlying resonances; thus the random-phase approximation is usually justified when dealing with averaged spectra. The extraction of average decay rates from linewidths in the regime of overlapping resonances is unjustified both on experimental and theoretical grounds.

4. Fluctuations in the Alignment Parameter, $A_0^{(2)}$

Having established that the linewidths in state-selected spectra are not a good measure of the dissociation rates, we need another way to explore the existence of state-to-state fluctuations in the rates. Direct time-resolved measurements require short photolysis and probe pulses, and thus typically yield rates averaged over a range of photolysis energies and summed over many product channels. However, time-dependent information can also be obtained indirectly from time-independent measurements *via* correlations in vector properties of fast dissociating molecules.[61–65] In order to relate the decomposition lifetimes to the rotational period of NO_2, we measured the state-specific alignment parameter $A_0^{(2)}$ of the NO fragment. Fluctuations in the value of $A_0^{(2)}$ as a function of E^E can signify fluctuations in the state-to-state rates.

Fluctuations in the rates of unimolecular reactions in the regime of isolated resonances have been inferred from linewidth fluctuations in the unimolecular reactions of formaldehyde and the methoxyl radical. Moore and co-workers have used Stark level crossing spectroscopy to examine the decomposition rates of single eigenstates in formaldehyde.[66] The observed rates varied by over one order of magnitude for states differing in energy by only fractions of a wavenumber; however, average values of the state-specific rate constants were reproduced by RRKM calculations with no adjustable parameters. More recently, Temps and co-workers have examined dissociation lifetimes

of individual rovibrational eigenstates of CH_3O in the vicinity of the classical barrier to $H + H_2CO$ fragmentation, using a triple resonance stimulated emission pumping (SEP) scheme combined with LIF.[67] Strong fluctuations in the state-specific linewidths with small variations in energy were observed. When the linewidths were converted to rates, the average rate were well reproduced by RRKM calculations.

A mathematical treatment of rotational alignment has been developed in several papers.[63–65,68] The alignment parameter $A_0^{(2)}$ characterizes the correlation between the vibronic transition moment μ in the parent and the fragment angular momentum J. $A_0^{(2)} = 0.8$ and -0.4 represent, respectively, the limiting cases of fragment J vector parallel and perpendicular to the parent vibronic transition moment.[61–65] In NO_2, the $1\,^2B_2 \leftarrow 1\,^2A_1$ transition moment lies in the molecular plane; thus, we expect $A_0^{(2)}$ to approach the limiting value of -0.4 for dissociation on a timescale fast compared with parent rotation.[22,35] Fig. 6 shows the reduction in $A_0^{(2)}$ expected for longer decomposition lifetimes at several NO_2 rotational temperatures. This calculation follows the treatment of Jonah,[69] and assumes a Boltzmann distribution of ground-state level populations. For each decomposition rate, as the temperature increases (*i.e.* the average period of rotation decreases) the $A_0^{(2)}$ value deviates further from its limiting value. Our measurements were carried out mostly at a parent rotational temperature of 4 K.

To obtain $A_0^{(2)}$ from our experimental LIF intensities, we follow the treatment of Dixon,[65] in which the integrated intensity $I(G, Q_i)$ of a rotational line in a photofragment fluorescence excitation spectrum is expressed as:

$$I(G, Q_i) = CSN_i\{b_0(G, Q_i) + b_1(G, Q_i)[\beta_0^2(02)(Q_i)]\} \quad (4)$$

where G refers to the specific photoysis-detection laser geometry, Q_i specifies the quantum numbers of the initial state which has population N_i, C is a constant, S is the rotational line strength factor, b_0 and b_1 are constants which depend on J, the rotational branch, and the specific laser-detection geometry, and $\beta_0^{(2)}(02)$ is related to the rotational alignment by $\beta_0^{(2)}(02) = 5/4A_0^{(2)}$. To determine $\beta_0^{(2)}(02)$ (and thus $A_0^{(2)}$) for a given product NO quantum state, we measure the $NO(A\,^2\Sigma^+ \leftarrow X\,^2\Pi_{1/2})$ LIF intensity for different geometries (I and II as denoted by Dixon)[65] on a fixed transition. This was accomplished by rotating the photolysis laser polarization, as described in Section 2.

As seen in Fig. 6, at $T_{rot} \approx 4$ K a sharp dependence of $A_0^{(2)}$ on decay lifetime τ is obtained for $\tau = 3$–15 ps. According to the $k(E)$ measurements of Ionov *et al.*,[14b] these lifetimes correspond to $E^E < 350$ cm^{-1}. However, at these excess energies only low J

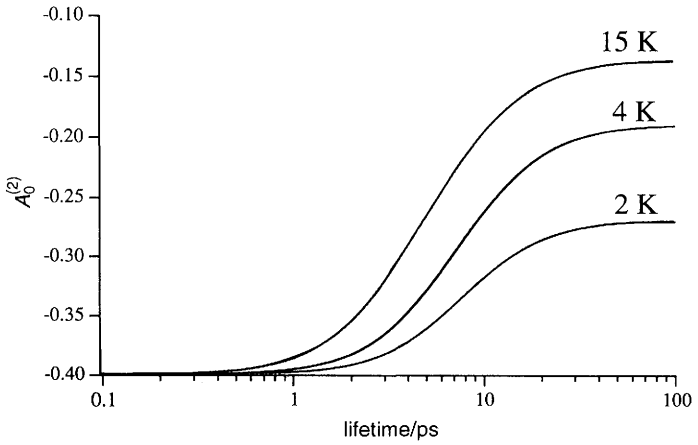

Fig. 6 Dependence of the alignment parameter $A_0^{(2)}$ on the dissociation lifetime of NO_2 at several rotational temperatures

levels of NO can be populated for which hyperfine depolarization is a prominent effect that markedly reduces the measured alignment.[63] The choice of E^E in our measurements represents a compromise between these two conflicting requirements [*i.e.* low E^E and high NO(J) states]; we therefore selected $E^E = 200$–$500\ cm^{-1}$ where the lifetimes are 2.5–1.4 ps, respectively,[14b] and $J = 10.5$ is the highest J level populated at the lowest E^E. Also, at $T_{rot} = 4$ K there is a larger change of $A_0^{(2)}$ with τ in this range than at lower temperatures (Fig. 6). Fig. 7 displays both a series of alignment measurements and a state-specific PHOFRY spectrum obtained by monitoring the $Q_{11}(10.5)$ transition of NO($^2\Pi_{1/2}$, $v = 0$). To correct for hyperfine depolarization we have measured $A_0^{(2)}$ for both $Q_{11}(10.5)$ and $Q_{11}(20.5)$ at higher E^E. In this normalization we assume that depolarization is not significant for $J_{NO} > 20.5$. This conclusion is confirmed by a study of NO_2 dissociation at $E^E = 3038\ cm^{-1}$,[22] where maximum alignment (*i.e.* $A_0^{(2)} \approx -0.4$) is obtained for NO($v = 1$, $J > 17.5$), while a clear reduction in $A_0^{(2)}$ is observed at lower J.

The $A_0^{(2)}$ values for selected peaks in the PHOFRY spectrum, corrected and uncorrected for hyperfine depolarization, are summarized in Table 1. The measured $A_0^{(2)}$ values fluctuate with energy in a reproducible manner. The corrected values range from *ca.* -0.3 at $E^E = 240$–$280\ cm^{-1}$ to *ca.* -0.35 at $E^E = 400$–$450\ cm^{-1}$, in agreement with the values reported by Miyawaki *et al.* in this energy region.[35] Similar average values and pattern of fluctuations were also obtained when monitoring NO($J = 6.5$) and correcting for depolarization. The error bars, $\pm 1\sigma$, represent the range of values obtained after many repetitions and during a period of several weeks. They refer to the precision of the absolute value for each $A_0^{(2)}$. Although the absolute values will sometimes vary from day to day, as a result perhaps of incomplete polarization or slight saturation effects, the relative values, which represent the fluctuations, are very reproducible and thus more robust than the absolute values.

There are several points worth discussing regarding the absolute values of $A_0^{(2)}$ and the nature and magnitude of their fluctuations. The limiting values of the averaged $A_0^{(2)}$ (-0.38, Fig. 6) is not reached even after correcting for depolarization. One reason for the deviation from the limiting value may be the simultaneous excitation of the perpendicular $1\,^2B_1 \leftarrow 1\,^2A_1$ transition, *e.g.* a 5% contribution from this transition can explain our reduced alignment. However, this is not considered very likely; all the experimental

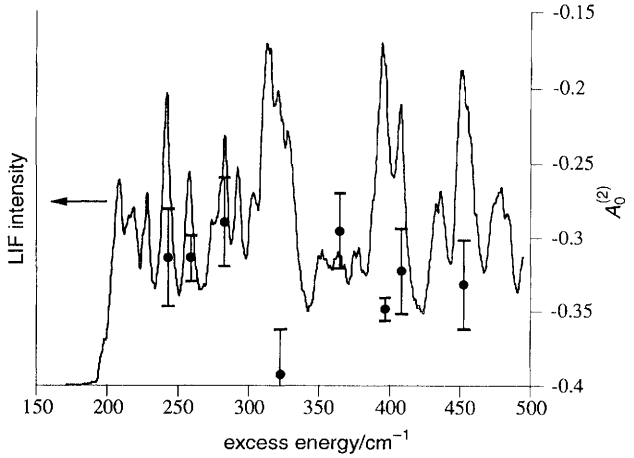

Fig. 7 One-photon PHOFRY spectrum (solid line) and measured $A_0^{(2)}$ values (filled circles) in the range $E^E = 200$–$500\ cm^{-1}$ obtained by monitoring the $Q_{11}(10.5)$ transition of NO($v = 0$). The $A_0^{(2)}$ values are corrected for hyperfine depolarization as described in the text; error bars correspond to $\pm 1\sigma$.

Table 1 Alignment parameters of $NO(^2\Pi_{1/2};\ v = 0;\ J = 10.5)$, and relative translational energies and velocities of fragments

E^E/ cm^{-1}	E_{tr}/ cm^{-1}	$A_0^{(2)}$ uncorrected	$A_0^{(2)}$ corrected[a]	v_{rel}/ Å ps^{-1}
242	41	-0.208 ± 0.022	-0.313 ± 0.035	3.1
258	57	-0.208 ± 0.010	-0.313 ± 0.015	3.6
282	81	-0.192 ± 0.020	-0.289 ± 0.030	4.3
326	125	-0.260 ± 0.020	-0.392 ± 0.030	5.3
364	163	-0.196 ± 0.017	-0.295 ± 0.026	6.1
379	196	-0.231 ± 0.005	-0.348 ± 0.008	6.7
408	207	-0.214 ± 0.019	-0.323 ± 0.028	6.9
452	251	-0.220 ± 0.020	-0.332 ± 0.029	7.6

[a] Corrected for hyperfine depolarization.

evidence points to the $^2B_2$ state as the only bright state efficiently coupled *via* the $1\,^2A_1$ state to the dissociation continuum. Moreover, the band positions of the $1\,^2B_1 \leftarrow 1\,^2A_1$ systems are well known,[70] and dispersed fluorescence studies show that highly localized $^2B_1$ vibronic states exist even at excitation energies as high as 22 000 cm^{-1} (*i.e. ca.* 3000 cm^{-1} below D_0).[71] Thus, any possible influence of the $^2B_1$ state would be localized to distinct known wavelengths characterizing absorption to this state.

Another probable cause for the reduced alignment is rotation of NO_2 prior to dissociation, which can change the plane of product NO rotation relative to the initial NO_2 molecular plane. Based on Fig. 6 and considering the average decomposition lifetime of NO_2 (*i.e.* 2.5–1.4 ps), we do not expect a significant reduction in $A_0^{(2)}$ at $E^E = 200$–500 cm^{-1} and $T_{rot} \approx 4$ K. However, we must also consider the timescale for the final $NO(^2\Pi_\Omega,\ J) + O(^3P_j)$ product separation as a function of internal energy, $E_{NO}(J) + E_O(j)$. For the reasons specified above, we preferentially monitor the highest NO states allowed energetically, which are states with low relative recoil velocity. The centre of mass (CM) translational energy available to the recoiling products, E_{tr}, is given by energy conservation:

$$E_{tr} = h\nu - D_0 - E_{NO}(J) - E_O(j) \tag{5}$$

At $E^E > 359$ cm^{-1}, $NO(^2\Pi_{1/2};\ J = 10.5)$ can be correlated with oxygen atoms in both the ground ($^3P_2$) and excited ($^3P_1$ or $^3P_0$) spin–orbit states. However, the average populations of $O(^3P_1)$ and $O(^3P_0)$ are small (even though state-to-state fluctuations in the spin–orbit populations are significant both as a function of E^E and the monitored NO quantum state),[21,33] and thus their contributions, which can further reduce E_{tr}, are ignored here. The values of E_{tr} calculated for $NO(^2\Pi_{1/2};\ J = 10.5) + O(^3P_2)$ are included in Table 1. We also calculate the NO–O recoil velocity, $v_{rel} = [2E_{tr}/\mu]^{1/2}$ (where μ is the reduced mass of the NO–O system), and these values are listed in Table 1 as well.

The recoil velocities, assuming dissociation solely to $NO(^2\Pi_{1/2},\ J) + O(^3P_2)$, are in the range 3.1–7.6 Å ps^{-1}. If long-range interactions are important for NO_2, as our NO rotational energy distributions and PST calculations indicate,[29] then some correlated orbital motion involving the NO–O complex may persist at large separations (*i.e.* for a longer timescales than indicated by the measured decay time τ), thereby altering the plane of rotation of NO relative to that of NO_2 at the time of excitation. This effect may reduce the alignment from the expected value based solely on $k(E)$.

A dependence of vector properties on the internal energy of the NO fragment has also been seen in measurements of the recoil anisotropy parameters, β_{rec}, in NO_2 photodissociation. These measurements, which yield in the limit of fast dissociation the direction of $\boldsymbol{v}$ relative to $\boldsymbol{\mu}$, show a reduction of β_{rec} with increasing $E_{NO}(J)$ both near

threshold,[36] and at higher E^E.[72] Thus, it appears that both $A_0^{(2)}$ and β_{rec} can be reduced when the relative separation velocity of the fragments is small. It will be interesting to verify this effect in molecules which dissociate from isolated resonances. For example, in the photodissociation of HCO, isolated resonances of varying widths are observed;[73,74] would the alignment and recoil anisotropy parameters for each resonance vary as a function of the monitored state of the CO product?

The reduction in the values of $A_0^{(2)}$ could also derive from preferential dissociation from high parent rotational levels. The rotational temperature in our experiments (4 K) was estimated from analysis of the structure in PHOFRY spectra right at D_0,[32] which yields values consistent with both direct LIF measurements of NO_2, and the rotational temperature of NO contaminant in the beam. Nevertheless, we also checked whether the reduction in alignment may arise from preferential contributions from high rotational states of NO_2 at the selected values of the photolysis energy for which the $A_0^{(2)}$ values were determined. To this end, we compared PHOFRY spectra obtained with 4% and 0.5% NO_2 in He (T_{rot} = 8–10 and 4 K, respectively). The peaks in the spectra did not change in shapes or relative magnitude; only some low-intensity 'background' peaks diminished in intensity in the more dilute samples. Our $A_0^{(2)}$ measurements were taken at prominent peaks which did not display a marked dependence of their structure on the dilution. We thus discount an effect due to preferential bias from high parent rotational levels on our results. In the experiments reported here, the 0.5% NO_2–He mixture was used because it gave colder T_{rot}.

Finally, we comment on the magnitude of the fluctuations in $A_0^{(2)}$. As mentioned above, the range of the average NO_2 decay lifetimes at $E^E = 240$–450 cm^{-1} is $\langle\tau\rangle$ = 1.4–2.5 ps. However, even an order of magnitude fluctuation about these lifetimes will correspond to only a modest change in $A_0^{(2)}$. Let $\langle\tau\rangle$ = 2.0 ps; the corresponding limiting value of $A_0^{(2)}$ is -0.38 (Fig. 6). An increase in τ by a factor of five will yield $A_0^{(2)} = -0.27$ for τ = 10 ps, whereas a decrease by a factor of five (to 0.4 ps) corresponds to the asymptotic value $A_0^{(2)} = -0.4$. Thus, under our experimental conditions, an order of magnitude fluctuation about the average lifetime will only lead to a change of $A_0^{(2)}$ between -0.4 and -0.27; moreover, our measurements are sensitive mainly to lifetimes longer than the average. In addition, with one-photon photolysis fluctuations tend to be further diminished due to incoherent averaging over several excited NO_2 rotational levels.[32,54] Thus, the magnitude of the fluctuations in the $A_0^{(2)}$ values reported here seems reasonable, and we believe that they reflect fluctuations in the unimolecular decay rates. Measurements using IR-visible double resonance excitations were also attempted, since they define the initial NO_2 state better; however, they resulted in poor signal to noise ratios.

5. Adiabaticity beyond the Transition State: Fluctuations in the NO Product State Distributions

In this section we comment on the relation between fluctuations and oscillations in PSDs and the statistical descriptions of unimolecular reactions. To test the validity of statistical theories, both microcanonical unimolecular reaction rates and PSDs are needed. In the absence of an activation barrier, as is common when the products are free radicals, such comparisons are more complex. The rate is usually calculated by finding variationally the dividing surface of minimum flux perpendicular to the reaction coordinate (the TS) for each E^E.[47] It is now well established that the TS moves inward from atop the centrifugal barrier as E^E increases.[43,47,75] Thus, in a triatomic molecule the TS levels will resemble those of a free rotor at low E^E, and be best described as hindered rotors or low-frequency bends at higher E^E.[38,55,75,76]

While rate calculations are rather straightforward even for a barrierless dissociation, the calculated PSDs must be examined more carefully. Near D_0, where the TS is very loose and its levels resemble those of the products, PST becomes the natural choice. This

theory apportions product populations as per the degeneracies of product quantum states, subject only to energy and angular momentum constraints.[48] As the TS tightens, but a barrier is absent, the situation is less clear and the issue of adiabaticity beyond the TS arises; *i.e.* do product states still exchange energy beyond the TS? In other words, how important are exit channel interactions beyond the TS? The current view is that product vibrations, especially those of a diatomic fragment, evolve rather adiabatically.[55,76] Rotational and spin–orbit states usually have small energy separations; do these evolve adiabatically, and if so where along the reaction coordinate does this happen? What are valid tests for statistical behaviour of the PSDs? We shall show that fluctuations and oscillation patterns in the PSDs provide insights into these important issues.

Although the PHOFRY spectra and NO product state distributions are complementary ways of viewing the same information, the latter sometimes better reveal patterns and regularities. We have obtained complete (*i.e.* rotational, vibrational and spin–orbit) state distributions of the nascent NO fragment for dissociation at specific excess energies in the range $E^E = 0$–3038 cm^{-1}.[29,33] In this section we examine the oscillations and fluctuations in the NO PSDs, compare the PSDs with statistical predictions, and examine the implications of the observations to the dissociation mechanism and to properties of the TS.

We focus here on NO rotational state distributions, and emphasize the excess energy region where the TS is expected to tighten signficantly. It appears that for each NO vibration, the TS is loose near its appearance threshold and tightens progressively as E^E increases.[14,31,35,38] Thus, we examine NO($v = 1$) rotational distributions from near threshold (at $E^E = 1876$ cm^{-1}) to 1160 cm^{-1} above this threshold. Displayed in Fig. 8 are NO($^2\Pi_{1/2}$, $v = 1$) rotational distributions for the two (A′, A″) Λ-doublet states of NO($^2\Pi_{1/2}$) obtained using one-photon excitation. Fig. 9 presents semilog plots of the distributions summed over Λ-doublet levels, compared with PST calculations.[29,48]

Inspection of each Λ-doublet level distribution reveals fluctuations in the rotational populations; however, the behaviour at low and high excess energies is different. Near the $v = 1$ threshold, rotational distributions for each Λ-doublet component fluctuate

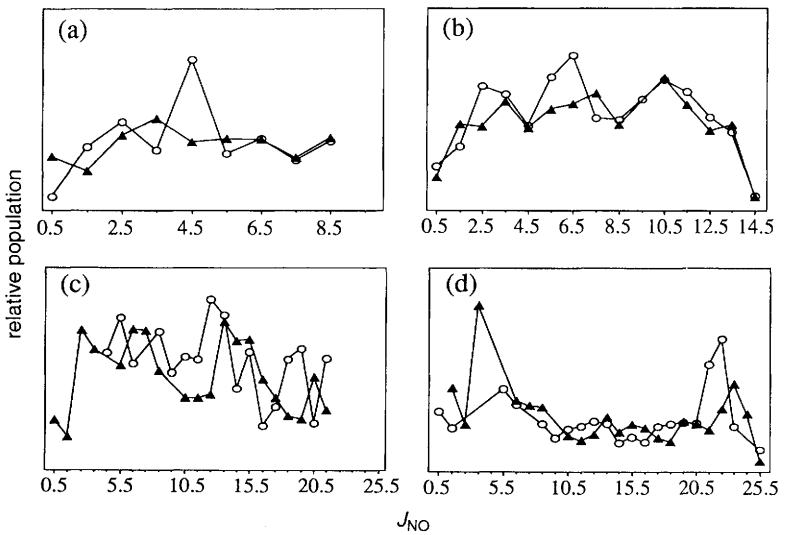

Fig. 8 NO($^2\Pi_{1/2}$; $v = 1$) rotational distributions obtained in one-photon dissociation of NO_2 at E^E = (a) 2061, (b) 2200, (c) 2700 and (d) 3038 cm^{-1}. The vibrational energy of NO($v = 1$) is 1876 cm^{-1}. Distributions for the two Λ-doublet states (A′, ▲ and A″, ○) are shown.

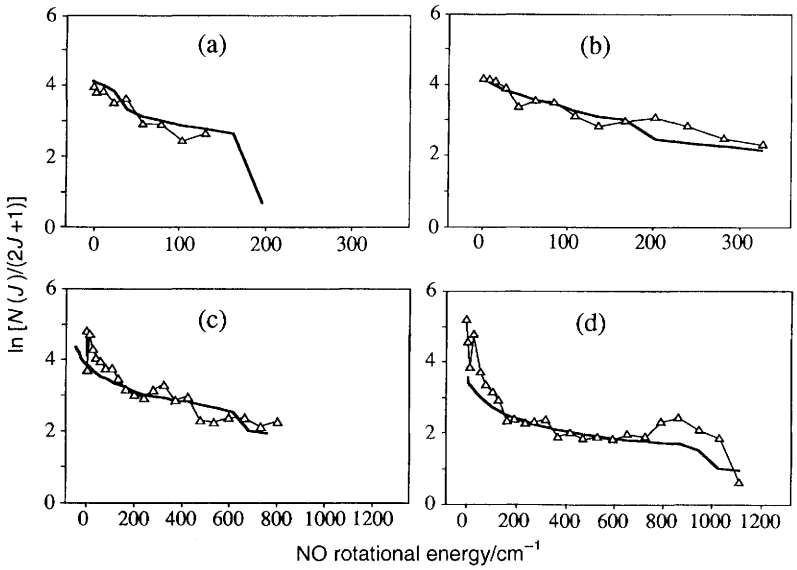

Fig. 9 Semilog plots of the rotational distributions presented in Fig. 8, summed over the Λ-doublet states of NO and compared with PST calculations (solid lines)

considerably, but the fluctuations are significantly diminished when summing over the Λ-doublet levels. These observations are also characteristic of NO($v = 0$) rotational state distributions at $E^E = 0$–400 cm^{-1},[29,32] and are consistent with near threshold PHOFRY spectra.[34,35] The $v = 1$ rotational distributions obtained at higher excess energies exhibit different behaviour. Here, the rotational distributions show pronounced oscillatory structures which are well reproduced for the two Λ-doublet states [as well as for spectra obtained when monitoring NO($^2\Pi_{3/2}$)],[29–32] and therefore are not diminished upon summation of the fine-structure states. This behaviour is particularly noticeable in Fig. 8(d) and 9(d) for NO($v = 1$) at 1162 cm^{-1} above its threshold, and also in NO($v = 0$) rotational distributions obtained at $E^E > 1800$ cm^{-1} (*e.g.* Fig. 3 and 4 of Ref. 31). The oscillatory structures depend sensitively on E^E. They are more easily identified in distributions obtained *via* one-photon excitation than in the double-resonance experiments, since fast fluctuating structures are averaged out by incoherent superpositions of distributions correlating with several parent rotational states.

It is instructive to compare the product state distributions with predictions of statistical models, and discuss the implications of our findings to the TS. Studies of the decompositions of NCNO[76–78] and CH_2CO[55,79,80] have shown good agreement with PST for diatom rotational distributions, indicating that the basic assumptions of the statistical theories are justified even in the fast dissociation of these small molecules. However, each quantum state of the diatomic fragment is typically correlated with many states of the other fragment, so averaging is inherent and no fluctuations or oscillations are observed.

The distributions shown in Fig. 9 all agree fairly well, on the average, with the predictions of PST. We have shown in previous work that the prominent oscillatory structures observed at high E^E can be modelled qualitatively by mapping bending-like wavefunctions associated with a tight TS into free rotor states of the NO fragment.[32,81] Why, then do the oscillations consistently cluster about the statistical predictions of PST, which assumes a very loose TS? This can be reconciled by recognizing two aspects of product evolution. First, the range of rotational excitations allowed in the Franck–

Condon mapping is a sensitive function of the TS bending angle and frequency.[81,82] The TS parameters used in the mapping calculations for NO_2 are based on *ab initio* calculations,[38,60] and they happen to give rise to rotational excitations that span the full range allowed by energy conservation at all excess energies studied.[32,81] The qualitative agreement observed with PST even at high excess energies thus reflects in part the specific geometry of the tight TS, and does not constitute a valid test for the looseness of the TS. This is an important recurrent theme; distributions which can be fit by a statistical model do not prove that such a model correctly describes the dissociation mechanism.

A second reason why PST-like distributions are observed even when the TS has tightened considerably is that exit-channel interactions beyond the TS can wash out oscillations and lead to population of all levels allowed by energy and angular momentum conservation. This effect is probably more important at lower energies, where the relative velocities of the recoiling products are small. Thus, the PSDs can be further modified beyond the TS *via* exit-channel interactions governed by a subtle interplay between the size of the energy quantum to be transferred and the relative recoil velocity. In barrierless reactions at low excess energies, the relative recoil velocities are small (see Table 1) and only low J levels (whose energy separation is small) are populated; thus, rotational energy transfer in the exit channel should be quite efficient. As the excess energy increases, the recoil velocity of the fragments increases, and the probability of rotational energy transfer in the exit channel decreases. Products in high rotational levels (whose energy separation is large) will undergo less efficient energy transfer, while products in low rotational levels will have higher recoil velocities and their evolutions may be well described by the sudden approximation. Previous studies have shown that the long-range attractive forces in NO_2 may extend to rather large O–NO internuclear separations,[29] thereby facilitating energy transfer. Thus, we expect that for each product vibration, at relatively low excess energies rotational energy transfer beyond the TS will be efficient and will smooth over oscillations arising from mappings of TS wavefunctions, resulting in a more PST-like behaviour. The oscillatory structures will remain prominent at higher excess energies where the sudden approximation is more justified. The NO($v = 1$) distributions suggest that the transition between the two regimes occurs between 400 and 1000 cm^{-1}. However, more work is clearly needed to explore the importance of long-range interactions beyond the TS.

In summary, the progressive tightening of the TS is revealed by the change in fluctuation patterns in the NO rotational state distributions from random to oscillatory as E^E increases. When the TS is loose (*i.e.* low E^E), it is not surprising that the rotational distributions are well described by PST. When the TS tightens and its levels become bending-like, agreement with PST may signify either efficient exit-channel interactions beyond the TS and/or mappings of wavefunctions of a TS whose geometry happens to produce PST-like distributions. In the case of NO_2, it is possible that both factors contribute to the average PST-like appearance of the rotational distributions, while the appearance of prominent oscillations whose shapes depend sensitively on E^E are the prime indicators of the tightening of the TS.

The similarity between oscillatory patterns obtained in rotational distributions of the two spin–orbit states of NO has led us to suggest that the spin–orbit distributions are fixed last, at long range, where the potential curves correlating with different spin–orbit pairs are close.[31] Recent *ab initio* calculations confirm this interpretation,[39] while explaining also why the lowest energy channel, $NO(^2\Pi_{1/2}) + O(^3P_2)$, is favoured.[33,39] Thus, the PSDs in NO_2 decomposition indicate that a hierarchy of adiabaticity exists. NO vibrations are fixed first, at the shortest O–NO separations, followed by the rotational distributions with their typical oscillatory patterns at higher E^E. The different electronic channels correlated with the different spin–orbit states of NO and O are determined only at large internuclear separations.[32]

6. Concluding Remarks

The unimolecular reaction of NO_2 exhibits fluctuations and oscillations evidenced in the PHOFRY spectra, the state-specific rates, and the PSDs. However, only those manifested in the state-selected PHOFRY spectra as fluctuations in the line positions and widths of spectral features obtained when monitoring different final states can be ascribed conclusively to overlapping resonances. Fluctuations in rates and PSDs have also been observed in dissociation from isolated resonances. For NO_2, comparisons between experimental and simulated PHOFRY spectra show that the effects of overlapping resonances are best revealed at moderate excess energies. Our simulations show that effects due to interference are most prominent when the overlap parameter $\langle\Gamma\rangle\rho$ is large (*i.e.* at high E^E) but the number of independent decay channels is modest (*e.g.* $n = 10$–30). In NO_2, this corresponds to the excess energy range $E^E = 200$–$3000\ cm^{-1}$, where most of our experiments were carried out.

It is intriguing that similar conditions (*i.e.* high E^E and modest n) are also required for the observation of prominent oscillations in the rotational distributions that depend sensitively on excess energy. These oscillatory structures derive from Franck–Condon mappings of bending-like TS wavefunction into rotational distributions, and have been interpreted as a manifestation of the tightening of the TS. Their experimental observation depends on the extent of exit-channel interactions, which are presently not taken into account in the simulations.[32,42] Energy transfer beyond the TS may wash out fluctuations and oscillations, particularly at low excess energies. Thus, agreement between the measured rotational distributions and PST predictions does not necessary imply a loose TS. Energy transfer beyond the TS and specific geometries of a tight TS may both lead to the appearance of PST-like rotational distributions. More work is clearly needed in order to understand long-range forces and exit channel interactions in simple bond-fission reactions.

We wish to thank our collaborators in these experiments, Martin Hunter, Dan Robie, Craig Bieler, Jenny Bates-Merlic, Uri Peskin and William H. Miller for their enthusiastic and valuable contributions to the understanding of the complex behaviour of NO_2 dissociation. We are indebted to Martin Hunter for providing the data used in Fig. 8 and 9. We benefited greatly from discussions with Curt Wittig, Howard Taylor, Jürgen Troe, Vladimir Mandelshtam and Reinhard Schinke. This research is supported by the US National Science Foundation, the Army Research Office and the Department of Energy, Basic Energy Sciences.

References

1 J. Miyawaki, K. Yamanouchi and S. Tsuchiya, *J. Chem. Phys.*, 1994, **101**, 4505.
2 (*a*) A. E. Douglas and K. P. Huber, *Can. J. Phys.*, 1965, **43**, 74; (*b*) A. E. Douglas, *J. Chem. Phys.*, 1966, **45**, 1007.
3 (*a*) D. Hsu, D. L. Monts and R. N. Zare, *Spectral Atlas of Nitrogen Dioxide 5530 to 6480 Å*; Academic Press, New York, 1978; (*b*) P. J. Brucat and R. N. Zare, *Mol. Phys.*, 1985, **55**, 277.
4 (*a*) H. Köppel, W. Domcke and L. S. Cederbaum, *Adv. Chem Phys.*, 1984, **57**, 59; (*b*) E. Haller, H. Köppel and L. S. Cederbaum, *J. Mol. Spectrosc.*, 1985, **111**, 377; (*c*) Th. Zimmermann, H. Köppel and L. S. Cederbaum, *J. Chem. Phys.*, 1989, **91**, 3934; (*d*) Th. Zimmermann, L. S. Cederbaum, H-D. Myer and H. Köppel, *J. Phys. Chem.*, 1987, **91**, 4446; (*e*) Th. Zimmermann, L. S. Cederbaum and H. Köppel, *Ber. Bunsen-Ges. Phys. Chem.*, 1988, **92**, 217.
5 J. C. D. Brand and P. H. Chiu, *J. Mol. Spectrosc.*, 1977, **75**, 1.
6 (*a*) G. Persch, H. J. Vedder and W. Demtröder, *Chem. Phys.*, 1986, **105**, 471; (*b*) G. Persch, H. J. Vedder and W. Demtröder, *J. Mol. Spectrosc.*, 1987, **123**, 356; (*c*) H. J. Vedder, M. Schwarz, H-J. Foth and W. Demtröder, *J. Mol. Spectrosc.*, 1983, **97**, 92; (*d*) G. Persch, E. Mehdizadeh, W. Demtröder, Th. Zimmermann, H. Köppel and L. S. Cederbaum, *Ber. Bunsen-Ges. Phys. Chem.*, 1988, **92**, 312.
7 (*a*) K. K. Lehmann and S. L. Coy, *J. Chem. Phys.*, 1985, **83**, 3290; (*b*) S. L. Coy, K. K. Lehmann and F. C. DeLucia, *J. Chem. Phys.*, 1986, **85**, 4297; (*c*) K. K. Lehmann and S. L. Coy, *Ber. Bunsen-Ges. Phys. Chem.*, 1988, **92**, 306.
8 J. L. Hardwich, *J. Mol. Spectrosc.*, 1985, **109**, 85.

9 R. E. Smalley, L. Wharton and D. H. Levy, *J. Chem. Phys.*, 1975, **63**, 4989.
10 (*a*) A. Delon and R. Jost, *J. Chem. Phys.*, 1991, **95**, 5686; 5700; (*b*) R. Georges, A. Delon and R. Jost, *J. Chem. Phys.*, 1995, **103**, 1732.
11 S. I. Ionov, H. F. Davis, K. Mikhaylichenko, L. Valachovic, R. A. Beaudet and C. Wittig, *J. Chem. Phys.*, 1994, **101**, 4809.
12 A. Delon, P. Dupre and R. Jost, *J. Chem. Phys.*, 1993, **99**, 9482.
13 (*a*) H. Gaedtke and J. Troe, *Ber. Bunsen-Ges. Phys. Chem.*, 1975, **79**, 184; (*b*) M. Quack and J. Troe, *Ber. Bunsen-Ges. Phys. Chem.*, 1975, **79**, 469; (*c*) H. Gaedtke, H. Hippler and J. Troe, *Chem. Phys. Lett.*, 1972, **16**, 177.
14 (*a*) G. A. Brucker, S. I. Ionov, Y. Chen and C. Wittig, *Chem. Phys. Lett.*, 1992, **194**, 301; (*b*) S. I. Ionov, G. A. Brucker, C. Jaques, Y. Chen and C. Wittig, *J. Chem. Phys.*, 1993, **99**, 3420; (*c*) C. Wittig and S. I. Ionov, *J. Chem. Phys.*, 1994, **100**, 4717.
15 C. Wittig, personal communication.
16 (*a*) H. Zacharias, M. Geilhaupt, K. Meier and K. H. Welge, *J. Chem. Phys.*, 1981, **74**, 218; (*b*) H. Zacharias, K. Meier and K. H. Welge, in *Energy Storage and Redistribution in Molecules*, ed. J. Hinze, Plenum Press, New York, 1983.
17 (*a*) M. Mons and I. Dimicoli, *Chem. Phys. Lett.*, 1986, **131**, 298; (*b*) M. Mons and I. Dimicoli, *Chem. Phys.*, 1989, **130**, 307.
18 M. Kawasaki, H. Sato, A. Fukuroda, T. Kikuchi, S. Kobayashi and T. Arikawa, *J. Chem. Phys.*, 1987, **86**, 4431.
19 K. Chen and C. Pei, *Chem. Phys. Lett.*, 1987, **137**, 361.
20 H-G. Rubahn, W. J. van der Zande, R. Zhang, M. J. Bronikowski and R. N. Zare, *Chem. Phys. Lett.*, 1991, **186**, 154.
21 (*a*) K. Yamanouchi, S. Takeuchi and S. Tsuchiya, *J. Chem. Phys.*, 1990, **92**, 4044; (*b*) J. Miyawaki, T. Tsuchizawa, K. Yamanouchi and S. Tsuchiya, *Chem. Phys. Lett.*, 1990, **165**, 168; (*c*) J. Miyawaki K. Yamanouchi and S. Tsuchiya, *Chem. Phys. Lett.*, 1991, **180**, 287.
22 N. Changlong, L. Hua and J. Pfab, *J. Phys. Chem.*, 1993, **97**, 7458.
23 V. P. Hradil, T. Suzuki, S. A. Hewitt, P. L. Houston and B. J. Whitaker, *J. Chem. Phys.*, 1993, **99**, 4455.
24 E. A. Rohlfing and J. J. Valentini, *J. Chem. Phys.*, 1985, **83**, 521.
25 G. E. Busch and K. Wilson, *J. Chem. Phys.*, 1972, **56**, 3626; 3638.
26 J. McFarlane, J. C. Polanyi and J. G. Shapter, *J. Photochem. Photobiol. A: Chem.*, 1991, **58**, 139.
27 J. A. Harrison, X. Yang, M. Rösslein, P. Felder and J. R. Huber, *J. Phys. Chem.*, 1994, **98**, 12260.
28 P. T. Knepp, A. C. Terentis and S. H. Kable, *J. Chem. Phys.*, 1995, **103**, 194.
29 (*a*) D. C. Robie, M. Hunter, J. L. Bates and H. Reisler, *Chem. Phys. Lett.*, 1992, **192**, 279; (*b*) M. Hunter, S. A. Reid, D. C. Robie and H. Reisler, *J. Chem. Phys.*, 1993, **99**, 1093; (*c*) M. Hunter, Ph.D. Thesis, University of Southern California, 1993.
30 S. A. Reid, J. T. Brandon, M. Hunter and H. Reisler, *J. Chem. Phys.*, 1993, **99**, 4860.
31 S. A. Reid, D. C. Robie and H. Reisler, *J. Chem. Phys.*, 1994, **100**, 4256.
32 S. A. Reid and H. Reisler, *J. Chem. Phys.*, 1994, **101**, 5683.
33 A. Sanov, C. R. Bieler and H. Reisler, *J. Phys. Chem.*, 1995, **99**, 13637.
34 (*a*) U. Robra, H. Zacharias and K. H. Welge, *Z. Phys. D*, 1990, **16**, 175; (*b*) U. Robra, Ph.D. Thesis, University of Bielefeld, 1984.
35 J. Miyawaki, K. Yamanouchi and S. Tsuchiya, *J. Chem. Phys.*, 1993, **99**, 254.
36 T. J. Butenhoff and E. A. Rohlfing, *J. Chem. Phys.*, 1993, **99**, 5460; 5469.
37 C. H. Chen, D. W. Clark, M. G. Payne and S. D. Kramer, *Opt. Commun.*, 1980, **32**, 391.
38 S. J. Klippenstein and T. Radivoyevitch, *J. Chem. Phys.*, 1993, **99**, 3644.
39 H. Katagiri and S. Kato, *J. Chem. Phys.*, 1993, **99**, 8805.
40 P-A. Elofson and E. Ljungstrom, *J. Chem. Phys.*, 1992, **165**, 323.
41 U. Peskin, H. Reisler and W. H. Miller, *J. Chem. Phys.*, 1994, **101**, 9672.
42 U. Peskin, W. H. Miller and H. Reisler, *J. Chem. Phys.*, 1995, **102**, 8874.
43 (*a*) D. M. Wardlaw and R. A. Marcus, *Adv. Chem. Phys.*, 1988, **70**, 231; (*b*) R. Marcus, *Philos. Trans. R. Soc. London, Ser. A*, 1990, **332**, 283, and references therein.
44 (*a*) M. Quack and J. Troe, *Ber. Bunsen-Ges. Phys. Chem.*, 1974, **78**, 240; **79**, 171; 1975, **79**, 469; 1977, **81**, 329; (*b*) J. Troek, *J. Chem. Phys.*, 1977, **66**, 4758; 1981, **75**, 226; 1983, **79**, 60; (*c*) J. Troe, *J. Phys. Chem.*, 1979, **83**, 114.
45 W. Forst, *Theory of Unimolecular Reactions*, Academic Press, New York, 1973.
46 P. J. Robinson and K. A. Holbrook, *Unimolecular Reactions*, Wiley, New York, 1972.
47 R. G. Gilbert and S. C. Smith, *Theory of Unimolecular and Recombination Reactions*, Blackwell, Oxford, 1990.
48 (*a*) P. Pechukas, J. C. Light and C. Rankin, *J. Chem. Phys.*, 1966, **44**, 794; (*b*) P. Pechukas and J. C. Light, *J. Chem. Phys.*, 1965, **42**, 3281; (*c*) J. C. Light, *Discuss. Faraday Soc.*, 1967, **44**, 14.
49 T. Ericson, *Ann. Phys.*, 1963, **23**, 390; *Phys. Rev. Lett.*, 1960, **5**, 430.
50 F. H. Mies and M. Krauss, *J. Chem. Phys.*, 1966, **45**, 4455.
51 F. H. Mies, *Phys. Rev.*, 1968, **175**, 164.

52 U. Fano, *Phys. Rev.*, 1961, **124**, 1866.
53 H. Feshbach, *Theoretical Nuclear Physics*, Wiley, New York, 1992.
54 S. A. Reid and H. Reisler, *J. Phys. Chem.*, 1996, **100**, 474.
55 W. H. Greene Jr., C. B. Moore and W. F. Polik, *Ann. Rev. Phys. Chem.*, 1992, **43**, 307.
56 R. D. Levine, *Ber. Bunsen-Ges. Phys. Chem.*, 1988, **92**, 222.
57 (*a*) W. H. Miller, R. Hernandez, C. B. Moore and W. F. Polik, *J. Chem. Phys.*, 1990, **93**, 5657; (*b*) R. Hernandez, W. H. Miller, C. B. Moore and W. F. Polik, *J. Chem. Phys.*, 1993, **99**, 950.
58 K. Someda, H. Nakamura and F. H. Mies, *Chem. Phys.*, 1994, **187**, 195.
59 J. Troe, *Chem. Phys.*, 1995, **190**, 381.
60 L. Harding, personal communication.
61 J. P. Simons, *J. Phys. Chem.*, 1987, **91**, 5378.
62 P. L. Houston, *J. Phys. Chem.*, 1987, **91**, 5388.
63 (*a*) C. H. Greene and R. N. Zare, *Ann. Rev. Phys. Chem.*, 1982, **33**, 119; (*b*) C. H. Greene and R. N. Zare, *J. Chem. Phys.*, 1983, **78**, 6741.
64 U. Fano and J. H. Macek, *Rev. Mod. Phys.*, 1973, **45**, 553.
65 R. N. Dixon, *J. Chem. Phys.*, 1986, **85**, 1866.
66 (*a*) W. F. Polik, D. R. Guyer and C. B. Moore, *J. Chem. Phys.*, 1990, **92**, 3453; (*b*) W. F. Polik, D. R. Guyer, W. H. Miller and C. B. Moore, *J. Chem. Phys.*, 1990, **92**, 3471.
67 A. Geers, J. Kappert, F. Temps and J. W. Weibrecht, *J. Chem. Phys.*, 1990, **93**, 1472; 1993, **99**, 2271; 1994, **101**, 3618; 3634.
68 R. N. Zare, *Angular Momentum.*, Wiley, New York, 1988.
69 C. Jonah, *J. Chem. Phys.*, 1971, **55**, 1915.
70 (*a*) A. E. Douglas and K. P. Huber, *Can. J. Phys.*, 1965, **43**, 74; (*b*) J. L. Hardwick and J. C. D. Brand, *Chem. Phys. Lett.*, 1973, **21**, 458.
71 J. B. Koffend, J. S. Holloway, M. A. Kwok and R. F. Heidner III, *J. Quant. Spectrosc. Radiat. Transfer*, 1987, **37**, 449.
72 H. Meyer, personal communication, 1995.
73 D. W. Neyer, X. Luo, I. Burak and P. Houston, *J. Chem. Phys.*, 1995, **102**, 1645.
74 (*a*) S. Williams, J. D. Tobiason, J. R. Dunlop and E. A. Rohlfing, *J. Chem. Phys.*, 1995, **102**, 8342; (*b*) J. D. Tobiason, J. R. Dunlop and E. A. Rohlfing, 1995, *J. Chem. Phys.*, **103**, 1448.
75 S. J. Klippenstein, in *Advances in Physical Chemistry: The Chemical Dynamics and Kinetics of Small Radicals*, ed. K. Liu and A. F. Wagner, World Scientific, 1995, in the press and references therein.
76 (*a*) H. Reisler and C. Wittig, *Ann. Rev. Phys. Chem.*, 1986, **37**, 307; (*b*) H. Reisler and C. Wittig, in *Advances in Kinetics and Dynamics*, ed. J. R. Barker, JAI Press, Greenwich, vol. 1, 1992.
77 (*a*) C. X. W. Qian, M. Noble, I. Nadler, H. Reisler and C. Wittig, *J. Chem. Phys.*, 1985, **83**, 5573; (*b*) C. Wittig, I. Nadler, H. Reisler, M. Noble, J. Catanzarite and G. Radhakrishnan, *J. Chem. Phys.*, 1985, **83**, 5581.
78 C. X. W. Qian, A. Ogai, H. Reisler and C. Wittig, *J. Chem. Phys.*, 1989, **90**, 209.
79 I. Garciamoreno, E. R. Lovejoy and C. B. Moore, *J. Chem. Phys.*, 1994, **100**, 8902.
80 (*a*) W. H. Green, I-C. Chen and C. B. Moore, *Ber. Bunsen-Ges. Phys. Chem.*, 1988, **92**, 389; (*b*) W. H. Green, I-C. Chen and C. B. Moore, *J. Chem. Phys.*, 1988, **89**, 314.
81 H. Reisler, H-M. Keller and R. Schinke, *Comments At. Mol. Phys.*, 1994, **30**, 191.
82 J. A. Beswick and W. M. Gelbart, *J. Phys. Chem.*, 1980, **84**, 3148.

Paper 5/06179B; *Received* 19*th September*, 1995